International Journal of Heat and Mass Transfer 271 (2026) 129352

Contents lists available at ScienceDirect

International Journal of Heat and Mass Transfer

journal homepage: www.elsevier.com/locate/hmt

An experimental study on the time dependence of diffusive mass transfer of single oxygen bubbles

Lotta Kursula *, Sayaka Takagi, Marko Hoffmann, Felix Kexel, Michael Schlüter *

Institute for Multiphase Flows, Hamburg University of Technology, Eißendorfer Straße 28, Hamburg, 21075, Germany

ARTICLE INFO

Dataset link: https://doi.org/10.15480/882.17032

This paper is dedicated to Professor Dieter Mewes on the occasion of his 85th birthday, in recognition of his enduring scientific contributions to multiphase flows and transport phenomena in chemical engineering.

Keywords:
Gas–liquid mass transfer
Sherwood number
PLIF
LSFM

ABSTRACT

In the vast majority of gas–liquid engineering applications, the liquid phase contains a range of dissolved gaseous species. These dissolved process gases transfer from the liquid phase to the gaseous phase counter-current to the typically desired mass transfer of gas to liquid. In process design, the resulting change in the composition of the gaseous phase is usually neglected, although a temporal change in the composition of the gaseous phase can directly influence the mass transfer performance over time. The current fundamental study quantifies the mass transfer performance of oxygen bubbles to liquid phases saturated with another gas. For this purpose, the oxygen mass transfer from a bubble to degassed, helium-, nitrogen-, argon- and carbon dioxide-saturated water is studied. Light Sheet Fluorescence Microscopy is used as imaging system for Planar Laser-induced Fluorescence measurements of dissolved oxygen concentration fields, delivering local instantaneous Sherwood numbers, diffusion coefficients and mass transfer coefficients. For the first time, the study showcases that the mass transfer performance from a gaseous dispersed to a liquid continuous phase is independent of time if mass transfer occurs in one direction only. If mass transfer occurs in both directions, the mass transfer performance of the dispersed phase is significantly lower and its time dependence higher to liquids containing gaseous species with high solubilities, such as carbon dioxide in water. Furthermore, the results suggest that applying intrinsic values, such as diffusion or mass transfer coefficients, obtained for binary systems in multicomponent systems can lead to high uncertainty.

1. Introduction

In gas–liquid multiphase reaction systems, such as bioreactors, the desired mass transfer most commonly occurs from the gaseous phase to the liquid phase. Namely, for processes utilising oxygen, the oxygen is supplied to the liquid phase via aeration followed by a dissolution of the bubbles. For a reliable process design, an accurate prediction of the dissolution behaviour, i.e., gas–liquid mass transfer is therefore vital. However, one phenomenon that is often not accounted for when modelling the gas–liquid mass transfer in such multiphase systems is the mass transfer of dissolved gaseous species from the liquid to the gaseous phase [1]. The liquid phase in reactors usually contains several other dissolved process gases that transfer from the liquid to the gaseous phase, analogously to the gas transferring to the liquid. As the partial pressures in the bubbles consequently change over time, the driving force of mass transfer decreases over time as well. This effect can, therefore, influence the mass transfer performance in multiphase systems. Yet, it is expected that the described phenomenon is only relevant in processes where gassing is realised with small bubbles; although small bubbles have a large volume-specific interfacial area, which is desirable for mass transfer, the partial pressures inside the bubbles can change rather quickly due to their small volume [2,3]. Consequently, small bubbles reach thermodynamic equilibrium with their environment faster than large bubbles. Hence, with decreasing bubble diameters, the global mass transfer performance becomes increasingly sensitive towards the dissolved gaseous species in the system [1]. In the current study, this effect is quantified on a local microscopic scale for diffusive mass transfer.

In a binary, purely diffusive system, the mass transfer of a component A can be described using the well-known Fick's second law of diffusion. Considering a gaseous bubble in a stagnant liquid, assuming isotropic diffusion,

$$\frac{\partial c_A}{\partial t} = \frac{1}{r^2} D_{A,B} \frac{\partial}{\partial r}\left(r^2 \frac{\partial c_A}{\partial r}\right) \tag{1}$$

is therefore valid. In Eq. (1), c_A is the concentration of species A, t is the time, r is the radial coordinate and $D_{A,B}$ is the diffusion

* Corresponding authors.
E-mail addresses: lotta.kursula@tuhh.de (L. Kursula), s.takagi@tuhh.de (S. Takagi), marko.hoffmann@tuhh.de (M. Hoffmann), felix.kexel@tuhh.de (F. Kexel), michael.schlueter@tuhh.de (M. Schlüter).

https://doi.org/10.1016/j.ijheatmasstransfer.2026.129352
Received 23 May 2026; Received in revised form 13 July 2026; Accepted 23 July 2026
Available online 30 July 2026
0017-9310/© 2026 The Authors. Published by Elsevier Ltd. This is an open access article under the CC BY license (http://creativecommons.org/licenses/by/4.0/).

coefficient of A in B. If the liquid phase contains one or more different dissolved gaseous species, the system becomes at least ternary. For example, when the volumetric mass transfer coefficient of oxygen is determined via dynamic degassing with nitrogen, the system consists of three species: oxygen as gaseous phase, the liquid phase and nitrogen dissolved in the liquid phase. In such a case, the dissolved gaseous species transfer from the liquid to the gaseous bubble and Eq. (1) does, strictly speaking, not apply any longer. This kind of mass transfer has been studied more for systems consisting of multiple liquids, using Maxwell–Stefan diffusion and Fick's law of diffusion [4–8], in comparison to systems where also gases are present, as in [9]. In a theoretical approach, Bothe and Druet [10] introduce a closure scheme for calculating multicomponent diffusion fluxes. The authors also provide a detailed review on the modelling of multicomponent mass transfer using Maxwell–Stefan or Fickian approaches [10]. Still, the experimental, but also theoretical, quantification of the impacts on the mass transfer performance of a gas to a liquid saturated with a different dissolved gaseous species remains incomplete. Matthes [1] and Muroyama et al. [11] studied the impacts on a global scale by quantification via the volumetric mass transfer coefficient. On a local scale, however, the impacts are yet to be quantified, although they have been observed in the shrinking behaviour of a single bubble [12] and modelled empirically [13].

In general, assuming sole resistance on the liquid side, the mass transfer performance of a process is quantified using the Sherwood number Sh

$$Sh = \frac{k_\mathrm{L} L}{D_\mathrm{A,B}}, \tag{2}$$

where k_L is the liquid-side mass transfer coefficient and L the characteristic length, for bubbles their diameter d_B. However, the parameters required in Eq. (2) are often not known. Also, the mass transfer performance is directly coupled to the diameter of the bubble, which implies that the change in diameter can directly be associated to the gas exiting the bubble. For multicomponent systems this assumption is not valid, as detailed above and by Hosoda et al. [13]. On a local bubble-scale, the change in mass transfer performance over time can be quantified by examining the local instantaneous Sherwood number $Sh_{t,\theta}$

$$Sh_{t,\theta} = -\frac{2}{H^*}\left(\frac{\mathrm{d}\xi}{\mathrm{d}r^*}\right)_{\mathrm{P},t,\theta} \tag{3}$$

over the Fourier number Fo

$$Fo = \frac{D_\mathrm{A,B} t}{r_\mathrm{B}^2}, \tag{4}$$

where θ is the polar angle with its origin at the north pole of the bubble. The Sherwood number in Eq. (3) is calculated from the gradient of the local, dimensionless concentration at the gas–liquid interface P

$$\xi(r^*) = \frac{c(r^*) - c_\infty}{c_{\mathrm{P},t_1} - c_\infty}, \tag{5}$$

with c denoting the mass concentration, and $r^* = \frac{r}{r_\mathrm{B}}$ for each point in time. Furthermore, in Eq. (3) H^* is the Henry's volatility coefficient

$$H^* = \frac{c_\mathrm{A,g}}{c_\mathrm{A,l}} \tag{6}$$

with $c_\mathrm{A,g}$ as the concentration of species A on the gaseous side and $c_\mathrm{A,l}$ as the concentration of A on the liquid side of the gas–liquid interface. An integration of the local instantaneous Sherwood number delivers the instantaneous Sherwood number Sh_t

$$Sh_t = \frac{1}{2}\int_0^\pi Sh_{t,\theta} \sin\theta \mathrm{d}\theta. \tag{7}$$

For diffusive mass transfer, meaning when the dissolved gas distributes spherically and isotropically, the local instantaneous Sherwood number in Eq. (3) equals the instantaneous Sherwood number in Eq. (7). A mean value of the instantaneous Sherwood numbers

$$Sh = \frac{1}{Fo}\int_0^{Fo} Sh_t \mathrm{d}Fo \tag{8}$$

equals the well-known global Sherwood number presented in Eq. (2) [14]. Furthermore, the instantaneous local Sherwood numbers defined in Eqs. (3) enable the calculation of local instantaneous liquid-side mass transfer coefficients $k_{\mathrm{L},t,\theta}$

$$k_{\mathrm{L},t,\theta} = \frac{Sh_{t,\theta} D_\mathrm{A,B}}{d_\mathrm{B}}. \tag{9}$$

According to Brauer and Mewes [14], the dimensionless mass transfer performance from a dispersed to a continuous phase has a time-independent zone, after which it decreases strongly. In diffusive cases, the time-independent zone is longer for increasing Henry's volatility coefficients and diminishes for small ones. In the current study, the time dependence of the diffusive mass transfer performance of small oxygen bubbles to water is studied. The impacts of dissolved gaseous species in the liquid phase are quantified on a local scale using Sherwood numbers, diffusion coefficients and mass transfer coefficients. For this purpose, diffusive oxygen mass transfer in a binary oxygen–water system, as well as ternary systems in which the water is saturated with nitrogen, helium, argon and carbon dioxide, respectively, are studied. Time-resolved Sherwood numbers are obtained from local dissolved oxygen concentration fields. The study showcases differences between the named liquid systems in the behaviour of the mass transfer performance over time quantitatively for the first time on a local scale.

2. Methods

Concentration fields of dissolved oxygen around single oxygen bubbles in water are measured using Light Sheet Fluorescence Microscopy (LSFM) as the imaging system for Planar Laser-induced Fluorescence (PLIF). The light sheet with a thickness of $\delta_\mathrm{LS} = 5$ µm in the focal point enables the measurement of time-resolved dissolved oxygen concentrations in a two-dimensional plane on a microscopic scale with a pixel pitch of $s = 0.27$ µm px^{-1}. For details on LSFM and PLIF, the reader is kindly referred to Kursula et al. [3] where the equipment and procedure of the concentration measurements are detailed and validated and measurement as well as calibration errors and uncertainties are discussed. Furthermore, Kursula et al. [3] summarise the image processing that is also applied in the current study. The following will focus solely on the experimental set-up and analysis, not on the measurement techniques and image processing.

2.1. Experimental set-up and procedure

The experimental set-up used in the current study is depicted in Fig. 1. The oxygen bubble is generated using a fused silica capillary (Fused Silica Capillary, *Postnova Analytics GmbH*, Germany) with an inner diameter of $d_\mathrm{I,c} = 2$ µm and pressurised oxygen in a standard spectroscopy cuvette (UV grade PMMA cuvette, *Kartell Spa*, Italy). The experiments are conducted at an ambient temperature of $T = (20 \pm 2)$ °C. The experimental procedure mainly follows the one described by Kursula et al. [3], where the procedure for the diffusive mass transfer of oxygen to physically degassed water is detailed. To quantify the effect of dissolved gaseous species in the liquid on the oxygen mass transfer performance, water is additionally saturated with different gases, namely nitrogen, helium, argon and carbon dioxide, and oxygen thereby removed prior to the measurements. The dissolved oxygen concentration fields are obtained via PLIF measurements. Therefore, an oxygen-sensitive fluorescent dye is mixed to the water, as in [3]. Due to the low concentration of the dye in water, $\zeta_\mathrm{dye} = 30$ mg L^{-1}, influences on the oxygen diffusion in water are considered negligible. To rule out influences on surface tension, the surface tension between the dye–water solution and air is measured using a drop volume tensiometer (DVT50, *Krüss*, Germany). The surface tension between the solution and air is $\sigma_\mathrm{sol,air} = (71.9 \pm 0.4)$ mN m^{-1} at $T = 26$ °C. Therefore, the dye is not expected to change the surface tension between water and oxygen. After saturating the water–dye solution with the respective

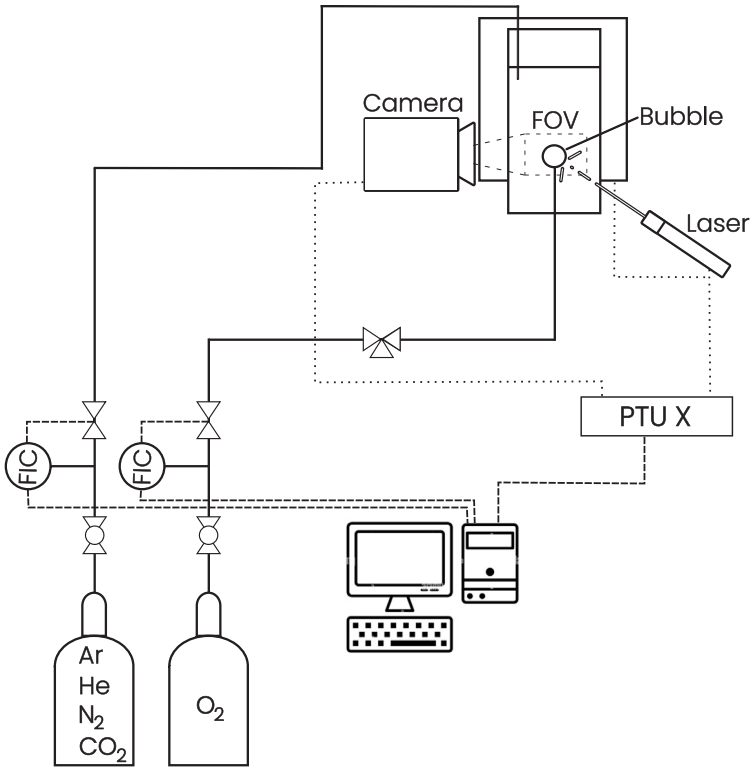

Fig. 1. Experimental set-up.

Table 1
Volumetric gassing ratios $\frac{\dot{V}_{O_2}}{\dot{V}_{gas}}$ and resulting dissolved oxygen concentrations $c^*_{O_2}\left(\frac{\dot{V}_{O_2}}{\dot{V}_{gas}}\right)$ used for the calibration curves.

ID Gas	Variable	1	2	3	4	5
Helium	$\frac{\dot{V}_{O_2}}{\dot{V}_{gas}}$	0	0.06	0.49	0.67	1
	$c^*_{O_2}\left(\frac{\dot{V}_{O_2}}{\dot{V}_{gas}}\right)$	0 mg L^{-1}	2.70 mg L^{-1}	22.40 mg L^{-1}	30.64 mg L^{-1}	45.67 mg L^{-1}
Nitrogen	$\frac{\dot{V}_{O_2}}{\dot{V}_{gas}}$	0	0.03	0.48	0.80	1
	$c^*_{O_2}\left(\frac{\dot{V}_{O_2}}{\dot{V}_{gas}}\right)$	0 mg L^{-1}	1.25 mg L^{-1}	21.55 mg L^{-1}	35.87 mg L^{-1}	45.67 mg L^{-1}
Argon	$\frac{\dot{V}_{O_2}}{\dot{V}_{gas}}$	0	0.06	0.48	0.80	1
	$c^*_{O_2}\left(\frac{\dot{V}_{O_2}}{\dot{V}_{gas}}\right)$	0 mg L^{-1}	2.50 mg L^{-1}	21.80 mg L^{-1}	36.63 mg L^{-1}	45.67 mg L^{-1}
Carbon dioxide	$\frac{\dot{V}_{O_2}}{\dot{V}_{gas}}$	0	0.12	0.41	0.68	1
	$c^*_{O_2}\left(\frac{\dot{V}_{O_2}}{\dot{V}_{gas}}\right)$	0 mg L^{-1}	5.53 mg L^{-1}	18.51 mg L^{-1}	31.03 mg L^{-1}	45.67 mg L^{-1}

one of the named gases, the liquid is transferred to the measurement cell and the measurement is conducted as described by Kursula et al. [3]. As a reference system for the diffusive mass transfer case, the data from [15] are used. The remaining data related to the current publication are available in [16]. Although the data for the binary, or reference, case are already published within the scope of a related publication, it is emphasised that the data acquisition took place alongside the ternary cases under identical experimental conditions and in an identical set-up. Except for the procedure for setting defined oxygen concentrations in the calibration and the physical degassing for oxygen removal instead of stripping, the experimental procedures followed the same protocol.

The calibration of the fluorescence intensity to a local dissolved oxygen concentration for the degassed system is detailed by Kursula et al. [3]. The calibration procedure in the ternary cases studied in the current study follows the same protocol, except for the method for setting defined dissolved oxygen concentrations in the liquid. In the cases where the water is saturated with one of the named gases, the defined dissolved oxygen concentrations are set by gassing the water with a gas mixture with defined ratios of oxygen and the respective other gas. The volumetric ratios then enable the calculation of the dissolved oxygen concentration

$$c^*_{O_2}\left(\frac{\dot{V}_{O_2}}{\dot{V}_{gas}}\right) = c^*_{O_2}\left(\frac{\dot{V}_{O_2}}{\dot{V}_{gas}} = 1\right)\frac{\dot{V}_{O_2}}{\dot{V}_{gas}} \tag{10}$$

once the liquid is saturated. Table 1 lists all volumetric gassing ratios and the resulting dissolved oxygen concentrations used for the calibration. For the measurements, the water is saturated with a respective gas, meaning that the measurements are conducted at ID = 1 in Table 1

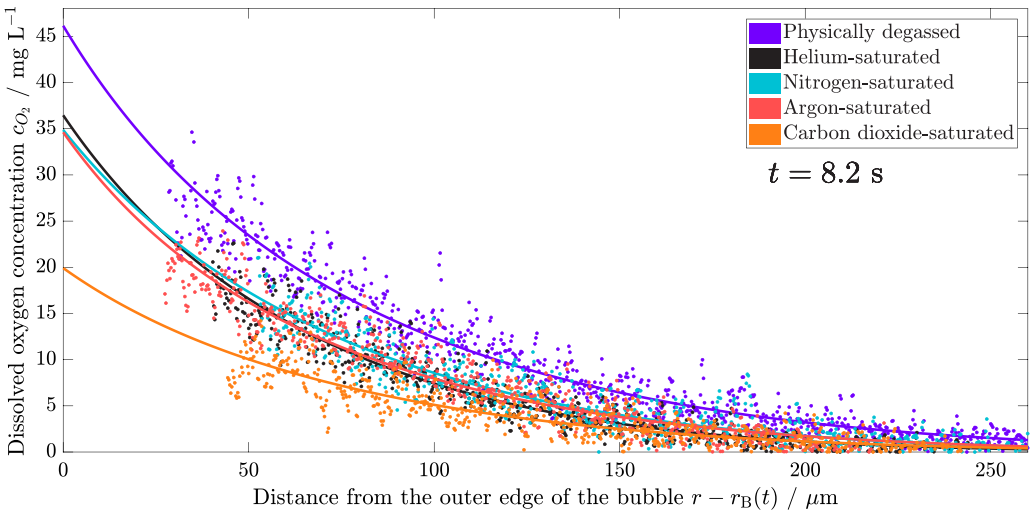

Fig. 2. Concentration of dissolved oxygen along the bubble equator in degassed (purple), helium-saturated (black), nitrogen-saturated (blue), argon-saturated (red) and carbon dioxide-saturated (orange) water at $t = 8.2$ s. Dots represent the measured data points from one measurement and curves the fitted curve from Eq. (12). (For interpretation of the references to colour in this figure legend, the reader is referred to the web version of this article.)

with no dissolved oxygen in the liquid phase initially. The resulting dissolved oxygen concentrations in the liquid cause a distinct quenching of the fluorescence, which is detected by the camera. By capturing the respective fluorescence intensities at defined dissolved oxygen concentrations, a calibration curve for each pixel can be obtained. Details on the chosen calibration curve

$$c_{O_2,i}(F) = \left(f_{a,i} K_{a,i} \left(\frac{F_{0,i}}{F_{0,i} - F} - \frac{1}{f_{a,i}} \right) \right)^{-1} \tag{11}$$

can be found in [3,17] and on the pixel-wise calibration procedure are provided by Kursula et al. [3].

2.2. Data analysis

The current study aims to calculate local instantaneous Sherwood numbers from the measured concentration data. Prior to the corresponding calculations, some processing and filtering of the data is necessary. These are explained in detail by Kursula et al. [3] and are therefore not reviewed here.

To obtain the gradient of the dimensionless concentration at the gas–liquid interface from Eq. (5), knowledge of the concentration curve in the vicinity of the interface is required. This can pose a challenge, because the concentrations in the vicinity of the bubble cannot be resolved reliably as a result of reflections of the laser from the gas–liquid interface. Therefore, concentrations in the vicinity of the bubble are filtered. The approach is described and justified in [3]. The solution of Fick's second law of diffusion

$$c_{O_2}(t,r) = \frac{r_B}{r} \operatorname{erfc}\left(\frac{r - r_B}{\sqrt{4 t D_{O_2,H_2O}}} \right) c^*_{O_2}, \tag{12}$$

where D_{O_2,H_2O} is the diffusion coefficient of oxygen in water and $c^*_{O_2}$ is the saturation concentration of oxygen in water, can be used for fitting. For binary systems with oxygen diffusion from the bubble to degassed water, it is sufficient to fit the diffusion coefficient only as the concentration at the interface stays constant. For systems where the liquid phase is saturated with another gaseous species, here helium, nitrogen, argon or carbon dioxide, the concentration at the interface changes with the changing partial pressure inside the bubble as the mass transfer progresses in both directions. Thus, the dissolved oxygen concentration at the gas–liquid interface $c^*_{O_2}$ is fitted for each point in time as well. Conventionally, a constant global diffusion coefficient is applied in Eq. (12). However, as discussed in [3], literature values of diffusion coefficients in general vary strongly and cannot be considered constant. The method applied in the current study yields instantaneous diffusion coefficients of oxygen in water. Fig. 2 shows the fitted curve and the measured data points after filtering for each liquid system exemplarily at time point $t = 8.2$ s along the bubble equator.

Finally, using Eqs. (3) and (5)–(8), the mean Sherwood numbers obtained at the bubble equator $\theta = \frac{\pi}{2}$ can be calculated. For calculating the dimensionless dissolved oxygen concentration using Eq. (5), $c_{P,t_1} = c^*_{O_2} = 45.67\,\text{mg L}^{-1}$ is taken. Physically, the concentration of dissolved oxygen at the interface must equal the saturation concentration of oxygen in water at the beginning of the mass transfer process, even if it could not be resolved temporally. Again, it is noted that for the diffusive mass transfer studied here, the local Sherwood number $Sh_{t,\theta=\frac{\pi}{2}}$ equals the instantaneous Sherwood number Sh_t (Eq. (7)). The Fourier number from Eq. (4) is calculated for each point in time for the respective bubble size.

3. Results and discussion

Table 2 summarises the diameters of the bubbles generated in the current study for each liquid system, along with the standard deviations of the three respective measurements. The diameters are denoted as maximal diameters, as the bubble generation is recorded as well. The bubble generation is included in the evaluations, because the mass transfer starts from the moment in which the gas exits the capillary. For the carbon dioxide-saturated system it should be noted that the maximal bubble diameter does not occur right after the generation. After the bubble generation, the bubble continued to grow, as the mass transfer of carbon dioxide from the water to the bubble is faster than the mass transfer of oxygen from the bubble to the water. Videos of the measurements are provided in S1 of the data supplements [16]. In these, the described effect of the growing bubble in carbon dioxide-saturated water can be observed.

3.1. Instantaneous diffusion coefficients

Fig. 3 shows the instantaneous diffusion coefficients fitted using Eq. (12) for the evaluated points in time together with a mean value for experimentally determined diffusion coefficient of oxygen in water $D_{O_2,H_2O} = 2 \times 10^{-9}\,\text{m}^2\ \text{s}^{-1}$ [18]. The confidence interval of the theoretical mean value is based on a standard deviation of 20% according to Cussler [5]. At first sight, it is immediately clear that the five liquid

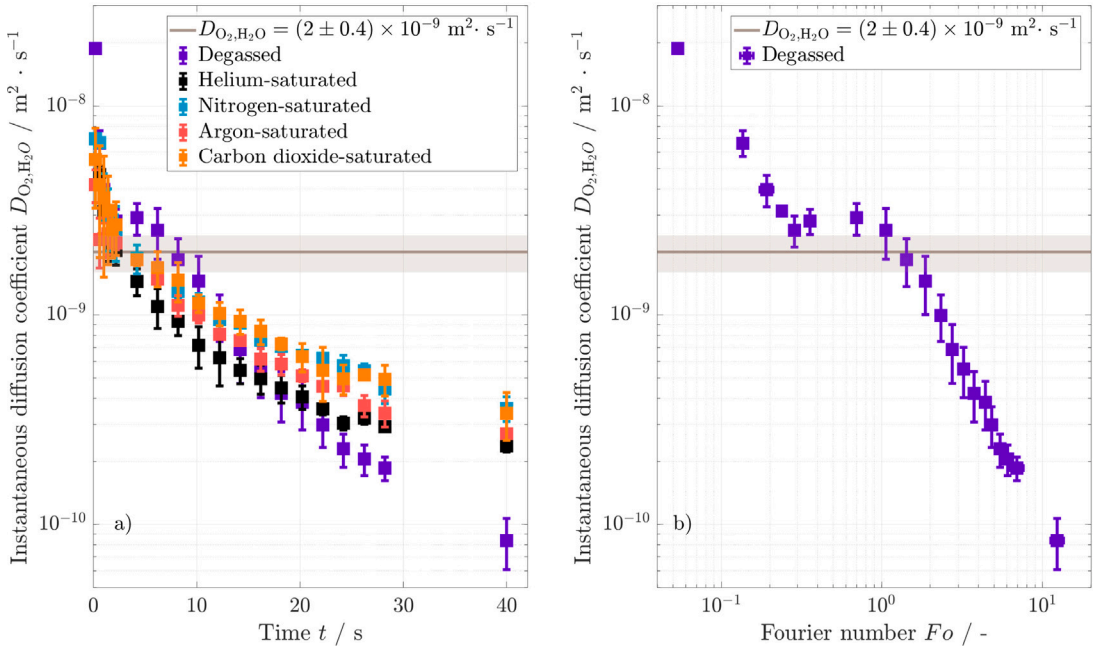

Fig. 3. Instantaneous diffusion coefficients of oxygen (a) in degassed (purple), helium-saturated (black), nitrogen-saturated (blue), argon-saturated (red) and carbon dioxide-saturated (orange) water over time and (b) in degassed (purple) water over the Fourier number. (For interpretation of the references to colour in this figure legend, the reader is referred to the web version of this article.)

Table 2
Maximal bubble diameters.

Degassing method	Maximal diameter d_B
Physically degassed	223 ± 4 µm (SD) [3]
Helium-saturated	220 ± 9 µm (SD)
Nitrogen-saturated	241 ± 4 µm (SD)
Argon-saturated	198 ± 6 µm (SD)
Carbon dioxide-saturated	231 ± 2 µm (SD)

systems studied in the current study yield different diffusion coefficients of oxygen in water. Furthermore, the diffusion coefficients determined in the current study emphasise the concentration-dependence of diffusion coefficients in general. When discussing the instantaneous diffusion coefficients in the liquid systems where the water is saturated with another gaseous species, it is good to note again that the solution of Fick's second law, shown in Eq. (12), is strictly speaking only valid for binary systems. Therefore, the diffusion coefficients obtained for the ternary systems shown in Fig. 3 should not be interpreted as intrinsic diffusion coefficients of oxygen, but rather should be used to recognise the difference in an effective diffusion coefficient of oxygen, or even just a fitting parameter, between the cases. Moving on, we now examine the diffusion coefficient of oxygen in degassed water, i.e., in a binary system of oxygen and water in more detail. In Fig. 3, it seems like the temporal evolution of the diffusion coefficient has three regions: an unstable start-up process at short times, a short stable region at intermediate times and, finally, a decrease in diffusivity at long times. The instabilities at short times until $t \approx 2$ s, or $Fo \approx 0.2$ in Fig. 3b, can be linked to the bubble generation. During that time period, the bubble is continuously supplied with oxygen and is growing rapidly, pushing the surrounding liquid away. Therefore, in this time period the mass transfer should not be taken as purely diffusive and the results should be handled with respective care. The decrease in diffusivity towards the end can be explained by the concentration-dependence of diffusion coefficients. With increasing concentration of dissolved oxygen in the water, the concentration gradient diminishes and the diffusion coefficient is no longer measurable [19]. Hence, the long-time decrease is not a physical change in diffusivity, such as in the first region, but a well-known measurement limitation leading to unmeasurable diffusivities. This phenomenon can explain why the decrease in the oxygen diffusion coefficient in the binary system is strongest; as the mass transfer progresses faster than in the other systems, the dissolved oxygen concentration in the liquid also increases faster. For the binary system of oxygen and degassed water, the three regions become even more clear when considering the diffusion coefficient as a function of the Fourier number, shown in Fig. 3b. For intermediate times, meaning approximately $0.2 < Fo < 1.5$, the diffusion coefficients in the binary system are slightly above the standard deviation of the theoretical diffusion coefficient of $D_{O_2,H_2O} = (2.0 \pm 0.4) \times 10^{-9}$ m^2 s^{-1}. An averaging of the fitted diffusion coefficients within the named range of Fourier numbers yields a diffusion coefficient of $D_{O_2,H_2O} = (2.6 \pm 0.5) \times 10^{-9}$ m^2 s^{-1} for oxygen in degassed water. Whilst the value is 30% higher than the stated literature value and exceeds the 20% bound from [5], the value still seems reasonable, especially considering the small scales. As discussed in [3], literature values of diffusion coefficients vary strongly. For example, at a temperature of $T = 20$ °C, the Stokes–Einstein equation yields $D_{O_2,H_2O} = 1.2 \times 10^{-9}$ m^2 s^{-1} and the Wilke–Chang correlation $D_{O_2,H_2O} = 2.2 \times 10^{-9}$ m^2 s^{-1}. The latter lays within the standard deviation of the value determined in the current study. Slight differences in the diffusion coefficient in the current study compared to other studies may also result from the fluorescent dye solved in the water, although this is considered unlikely due to the low concentration of the dye. Further deviations can result from the stated temperature range of $T = (20 \pm 2)$ °C during the experiment, as the diffusion coefficient is temperature sensitive. It is also emphasised that the authors denote the diffusion coefficient of $D_{O_2,H_2O} = 2 \times 10^{-9}$ m^2 s^{-1} as a mean experimental value [18] rather than a strictly fixed one. Considering these arguments, the obtained diffusion coefficient of $D_{O_2,H_2O} = (2.6 \pm 0.5) \times 10^{-9}$ m^2 s^{-1} is satisfying and validates the measurements.

For engineering applications, the differences in the diffusion coefficient and its temporal evolution mean that the application of intrinsic diffusion coefficients originally obtained for binary systems in multi-component systems should be considered carefully. For intermediate times, i.e., the time period in which the instabilities of the start-up process are overcome but where the concentration in the liquid does not cause the diffusion coefficient to diminish, the diffusion coefficients

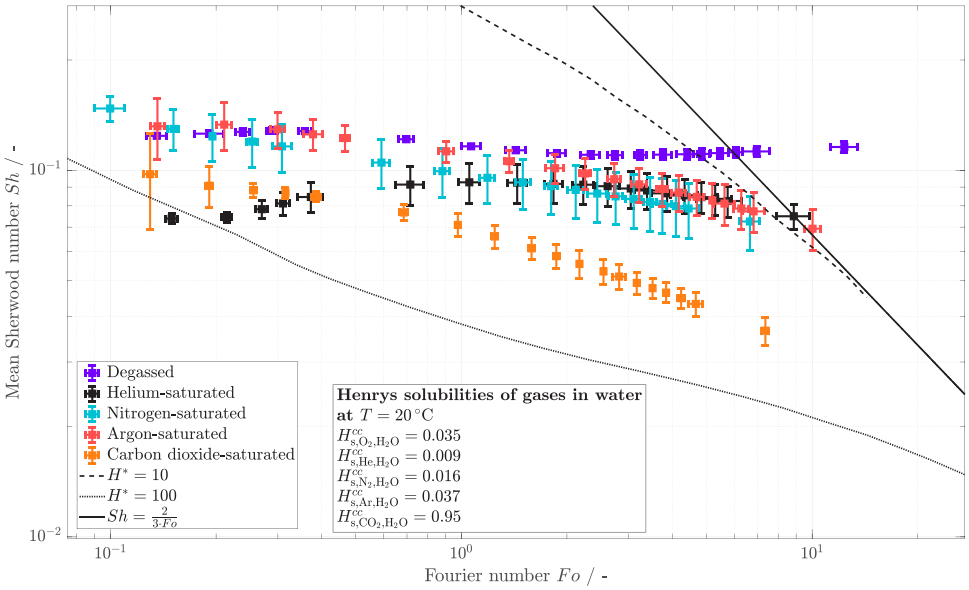

Fig. 4. Mean Sherwood number over the Fourier number for an oxygen bubble in degassed (purple), helium-saturated (black), nitrogen-saturated (blue), argon-saturated (red) and carbon dioxide-saturated (orange) water with upper boundary $Sh = \frac{2}{3Fo}$ (solid line) and theoretical values for $H^* = 10$ (dashed line) and $H^* = 100$ (dotted line) from [14]. (For interpretation of the references to colour in this figure legend, the reader is referred to the web version of this article.)

in the degassed system are roughly 60% higher than the fitting parameters representing somewhat effective diffusion coefficients in the ternary systems. It is emphasised again that the diffusion coefficients obtained for the ternary systems should not be interpreted as diffusion coefficients of oxygen, but are only utilised to encourage consideration of all species in the system. If the mass transfer is sensitive towards dissolved gaseous species in the liquid, a deviation in the diffusion coefficient can lead to erroneous calculations. The mass transfer performance from larger bubbles is not sensitive towards dissolved species in the liquid [2]. However, mass transfer from small bubbles is sensitive in this regard, meaning that, as also shown in the current study, the diffusion coefficients are sensitive. Thus, the application of intrinsic binary diffusion coefficients in equations valid for binary systems, such as Eqs. (1) and (12), should be handled with care.

3.2. Sherwood numbers

In Fig. 4, the evolution of the mean Sherwood numbers obtained at the bubble equator $\theta = \frac{\pi}{2}$ over the dimensionless time Fo is shown. It should be noted that the Fourier numbers shown in Fig. 4 are calculated using the mean diffusion coefficient of oxygen in water from [18] and not using the instantaneous diffusion coefficients presented above. Using a constant diffusion coefficient ensures the comparability of the results with literature, as diffusion coefficients are commonly considered constant. Furthermore, the upper limit for large times of the Sherwood number, assuming a constant volume of the dispersed phase, and the expected curves of the Sherwood numbers for Henry's volatility coefficients $H^* = 10$ and $H^* = 100$ between the dispersed and continuous phase from [14] are shown as a comparison. In the current study, Henry's volatility of oxygen and water is $H^* = 28.6$ at the given temperature. As the measured data fit well between the literature values, the measurements seem valid. Furthermore, Table 3 summarises the mean Sherwood numbers obtained with Eq. (8) for the whole Fourier number period.

Brauer and Mewes [14] define three regions of mass transfer performance. First, there is a short time period in which the mean Sherwood number decreases in time, meaning the mass transfer performance is time-dependent. This region is followed by a time-independent region where the mean Sherwood number is constant. For diffusive systems, this region is shorter for decreasing Henry coefficients H^* between the dispersed and continuous phase, as visible in Fig. 4 for Henry coefficients $H^* = 10$ and $H^* = 100$. Towards the end of the mass transfer the Sherwood number starts to decrease again and the mass transfer is, again, time-dependent [14]. Before discussing the mean Sherwood numbers in detail, it is necessary to recall that the bubble growth in the measurements of the current study causes instabilities until $Fo \approx 0.4$. This can explain the rather large spread of the mean Sherwood numbers until then.

Table 3
Sherwood numbers averaged over the Fourier number.

Degassing method	Mean Sherwood number Sh / -
Physically degassed	0.116 ± 0.004 (SD)
Helium-saturated	0.076 ± 0.006 (SD)
Nitrogen-saturated	0.073 ± 0.012 (SD)
Argon-saturated	0.069 ± 0.009 (SD)
Carbon dioxide-saturated	0.037 ± 0.003 (SD)

The mass transfer performance of oxygen in the binary system of oxygen and water remains quite constant over time. In the ternary cases, on the other hand, the mass transfer performance starts to decrease after some time. Contrary to the constant mass transfer performance in the binary system, the time-dependent behaviour is also described by Brauer and Mewes [14]. In the current study, using dimensionless numbers, a difference between the gaseous phases used to saturate the water cannot be identified, except for the carbon dioxide-saturated system, see Table 3. Compared to the degassed system, the mean Sherwood number in the carbon dioxide-saturated system is 68% lower. Comparing the binary case to the remaining systems, the difference is roughly 50%. The markable difference in oxygen mass transfer performance in the carbon dioxide-saturated water may be caused by density-driven convection, as already observed for diffusive carbon dioxide mass transfer [20–22]. If the mass transfer of carbon dioxide from the water to the bubble is enhanced by density-driven convection, it is conceivable that the mass transfer of oxygen is inhibited resulting in lower Sherwood numbers. However, an indication for a buoyancy-driven flow cannot be identified from the measurements, as visible in the supplemented video [16]. The differences between the other three gases used for saturating the water are not as prominent. It should be reviewed that the Fourier number depends on the diameter of the

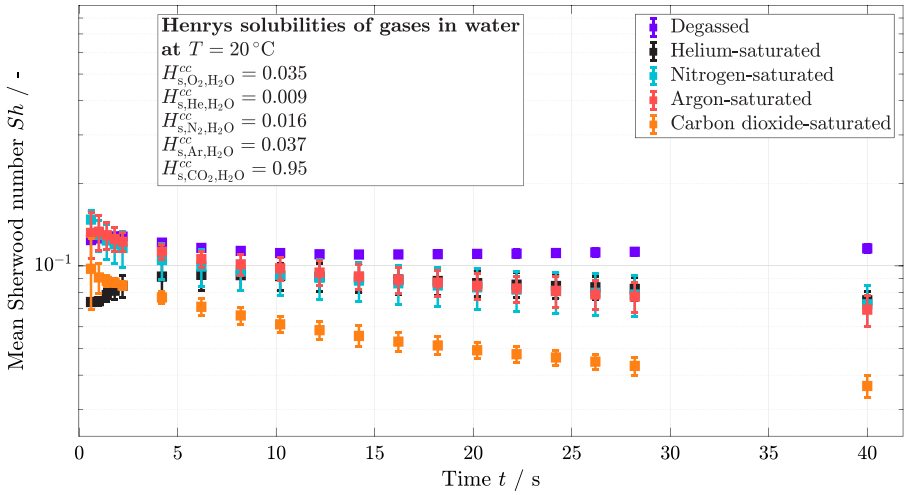

Fig. 5. Mean Sherwood number over time for an oxygen bubble in degassed (purple), helium-saturated (black), nitrogen-saturated (blue), argon-saturated (red) and carbon dioxide-saturated (orange) water. (For interpretation of the references to colour in this figure legend, the reader is referred to the web version of this article.)

Table 4
Henry's solubility coefficients of gases in water at $T = 20\,°C$.

Gas	Henry's solubility coefficient H^{cc}_{s,i,H_2O} / -
Oxygen	0.035
Helium	0.009
Nitrogen	0.016
Argon	0.037
Carbon dioxide	0.95

bubble. As the diameter depends on the mass transfer from and to the bubble, the dimensionless time passes differently from the physical time for the five cases presented here. When considering the Sherwood number a function of the physical time in Fig. 5, the link between the solubility of the respective dissolved gaseous species and the differences in the evolution of the mass transfer performance can be verified at least for carbon dioxide. It is noted that the solubility here is not related to the volatility H^* of the dispersed phase, which also governs the time dependence of mass transfer, but should be considered a distinct mechanism related explicitly to the other dissolved gaseous species. Again, the carbon dioxide-saturated system can easily be identified as the system where the mass transfer performance of oxygen is lowest. For the remaining liquid systems, the mass transfer performance of oxygen in the argon-saturated water for long times seems to be lowest, although the difference is not high enough to claim it statistically significant. The solubilities of oxygen, nitrogen and argon are in a similar range, whilst the solubility of helium is very low, as listen in Table 4. However, despite the solubility of helium is significantly lower than that of oxygen, nitrogen or argon, the differences in solubility between these four gases are negligible compared to the solubility of carbon dioxide. This means that whilst the differences in the Sherwood number can be linked to the solubility of the dissolved gaseous species, said differences remain small and negligible for systems where the solubility of the solved gaseous species is in a similar order of magnitude as the one the of the gaseous dispersed phase, here helium, nitrogen or argon. If the liquid is saturated with a gaseous species with a very high solubility, such as carbon dioxide, the Sherwood number is, however, influenced significantly. Considering the very high solubility of carbon dioxide compared to the other gases, it seems valid that the Sherwood numbers in the systems where the liquid is saturated with helium, nitrogen or argon are indistinguishable. In any case, the Sherwood numbers are lower than those in the binary system and show a different trend.

At first glance, it may seem counter-intuitive that the mass transfer performance in the binary system stays constant whilst decreasing in the remaining systems. An explanation can be provided by examining Eqs. (3) and (5) and by revisiting the physical mechanisms. If gases are solved in the liquid phase, as it is usually the case, the dissolved gaseous species transfers from the liquid phase to the gaseous phase, here from water to the oxygen bubble. With progressing mass transfer and time, the partial pressure of oxygen in the bubble decreases. For Eq. (5) this means that the denominator stays constant whilst the numerator decreases. Therefore, also the gradient of the dimensionless concentration $\xi_{O_2}(r^*)$ at the gas–liquid interface decreases over time and hence the Sherwood number calculated with Eq. (3). However, if the liquid does not contain any gases, such as the degassed water in the current study, the partial pressure of oxygen in the bubble does not decrease, as no mass transfer to the bubble takes place. With a constant oxygen partial pressure in the bubble, the concentration at the gas–liquid interface stays constant over time and the local Sherwood number calculated with Eq. (3) does not change. Fig. 6 shows the dimensionless dissolved oxygen concentrations ξ_{O_2} for all cases over the dimensionless radius r^* for four points in time. For the degassed case, the gradient at the interface barely changes, whilst decreasing in all other liquid systems. The results in Figs. 4 and 6 clearly show that the time dependence of the gas–liquid mass transfer performance is caused by the mass transfer from the liquid phase to the gaseous phase. At this point, it is good to note that Brauer and Mewes [14] and Streicher and Schügerl [23] link the time dependence of the mass transfer performance to a changing composition of the dispersed phase. However, our study distinctly considers a case in which the composition of the dispersed phase does not change with time for the first time.

It is furthermore worth noting that the Sherwood number in the physically degassed water exceeds the theoretical upper bound $Sh = \frac{2}{3Fo}$. As mentioned above, the upper bound is derived for mass transfer with a constant volume of the dispersed phase. Assuming a constant volume of the dispersed phase while an ongoing mass transfer out of the dispersed phase implicitly equals the assumption of an equimolar mass transfer in and out of the dispersed phase. Such an equimolar mass transfer in and out of the dispersed phase naturally leads to a changing composition of the dispersed phase. In the experiments of the current study, the volume change of the bubble is the highest for the oxygen bubble in the physically degassed water. For this reason and because of the constant partial pressure of oxygen in the bubble, the Sherwood number can exceed the theoretical upper bound. Whilst the assumption of a constant volume does not discredit the results for

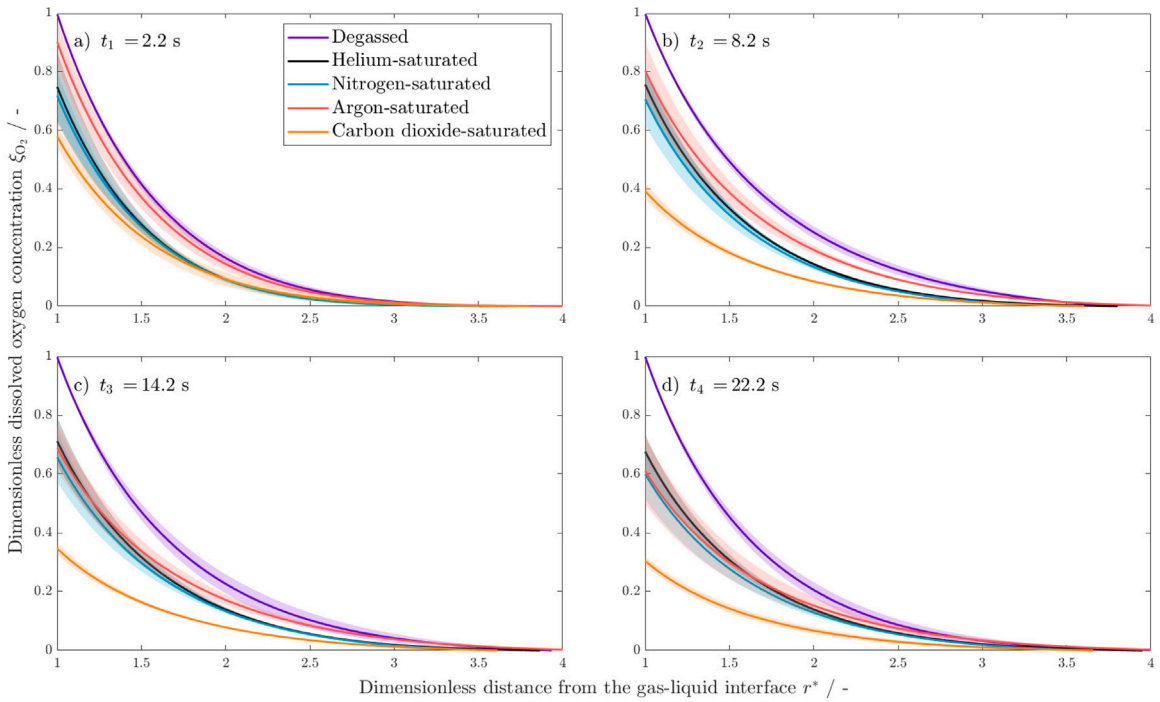

Fig. 6. Dimensionless dissolved oxygen concentration ξ_{O_2} at $\theta = \frac{\pi}{2}$ over the dimensionless radius r^*, with $r^* = 1$ being the gas–liquid interface, in the concentration boundary layers for degassed (purple), helium-saturated (black), nitrogen-saturated (blue), argon-saturated (red) and carbon dioxide-saturated (orange) water. (a) $t_1 = 1.8$ s (b) $t_2 = 4.2$ s (c) $t_3 = 14.2$ s and (d) $t_4 = 22.2$ s. (For interpretation of the references to colour in this figure legend, the reader is referred to the web version of this article.)

the ternary systems, differences from the theory can yet be explained with the assumption. Directly, the changing volume of the bubbles only affects the Fourier number. The local Sherwood number remains largely unaffected, as it is calculated from the gradient of the dimensionless concentration over the dimensionless radius, see Eq. (3). A decreasing diameter over time results in a faster progression of dimensionless time, i.e. Fourier number, and vice versa. Therefore, the changing diameter of the bubbles can induce a horizontal shift of the Sherwood numbers in Fig. 4, strictly speaking resulting in individual upper bounds for each ternary system. However, the main interpretations remain as stated despite the changing diameter. This line of argumentation also applies to the differences in bubble sizes shown in Table 2. Although the differences in bubble sizes somewhat affect the Fourier number and thus the dimensionless temporal evolution of the mass transfer performance, the dimensionless mass transfer performances are still comparable. For significantly larger bubbles, e.g. sizes within the macroscopic scale, this assumption may have to be reconsidered.

The primary limitation that may result in large uncertainties in the Sherwood number emerges from the fitting of the concentration at the gas–liquid interface in the ternary cases. In Fig. 6, the standard deviations resulting from three measurements are shown. These cannot directly be linked to the uncertainty emerging from the fitting, because also other factors, such as temporal matching of the three measurements as detailed in [3], influence the fitted function. Yet, the standard deviations of the concentration are largest at the interface and are thus propagated to the local Sherwood numbers. Therefore, the standard deviations emerging from three respective measurements are deemed sufficient to assess the sensitivity of the Sherwood number toward errors in the concentration and its gradient at the interface. The resulting errors in the Sherwood number for the ternary systems shown in Table 3 are all within a range from 8 to 16%, which is considered acceptable as the results seem overall plausible after the discussion above.

3.3. Instantaneous liquid-side mass transfer coefficients

As mentioned in Section 1, Eq. (9) enables the calculation of instantaneous liquid-side mass transfer coefficients $k_{L,t,\theta}$. Fig. 7 shows the liquid-side mass transfer coefficients over time. The liquid-side mass transfer coefficients are calculated according to Eq. (9) using instantaneous Sherwood numbers and effective diffusion coefficients from Fig. 3. The liquid-side mass transfer coefficients in general show a similar trend as the diffusion coefficients discussed in Section 3.1. Using the same line of argumentation as in Section 3.1 neglecting short and long times, the liquid-side mass transfer coefficient of oxygen in water for the binary system can be estimated with $k_L = 1.51 \times 10^{-6}$ m s^{-1}. For the ternary systems it is, again, difficult to determine one representative value. Still, the liquid-side mass transfer coefficients in the ternary systems are roughly halved compared to the binary system in the respective period of time. Of course, there are also other methods to calculate the liquid-side mass transfer coefficient, for example in accordance with the two-film theory [24] or from the molar balance [25]. However, the aim of the current study is to introduce and emphasise the differences of cases where mass transfer occurs in one direction versus when it occurs in two directions. The mass transfer coefficients again show that applying intrinsic values obtained in binary systems and using equations valid for binary systems on multicomponent problems should be considered carefully.

4. Conclusion

In this study, the local diffusive mass transfer of oxygen to water is quantified using the local instantaneous Sherwood number. For the first time on a local scale, we show quantitatively with experiments that the Sherwood number, i.e., the mass transfer performance of a dispersed phase is independent of time when mass transfer occurs in one direction only. Moreover, the results show that the performance and time dependence of the mass transfer of a gaseous dispersed phase can be linked to the solubility of the gaseous species dissolved in the liquid phase. In this

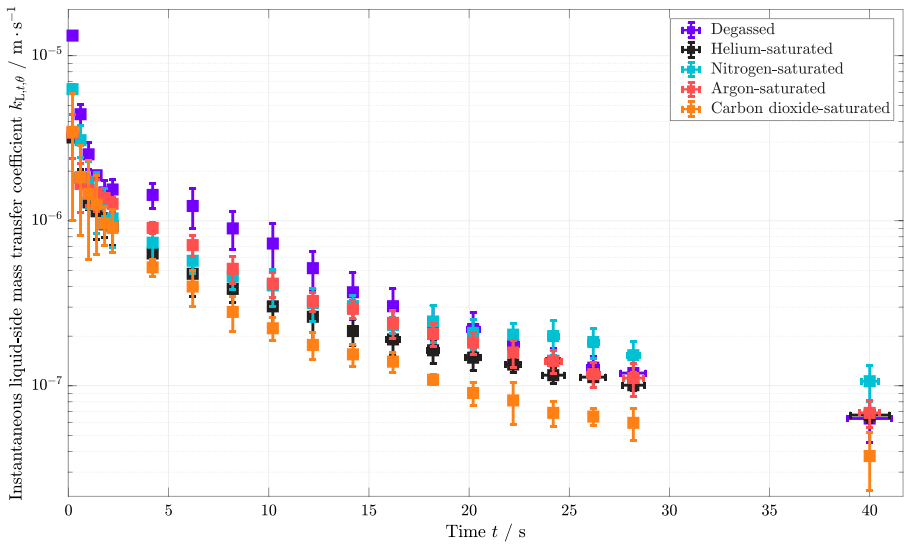

Fig. 7. Instantaneous liquid-side mass transfer coefficients of oxygen in degassed (purple), helium-saturated (black), nitrogen-saturated (blue), argon-saturated (red) and carbon dioxide-saturated (orange) water over time. (For interpretation of the references to colour in this figure legend, the reader is referred to the web version of this article.)

study, the oxygen mass transfer performance is by far the lowest and shows the highest dependence of time in water saturated with carbon dioxide, a gas with a very high solubility in water. Furthermore, the obtained data suggest that intrinsic values, such as the mass transfer and diffusion coefficients, from binary systems are not applicable on systems with several dissolved gases and small bubbles, although this is commonly assumed in engineering applications. The effect is expected to be especially relevant for small bubbles as their small volume can reach equilibrium with their environment faster than the larger volume of larger bubbles. Therefore, the phenomena presented in the current study become particularly relevant for modern applications utilising micro-spargers, aiming for high interfacial areas and mass transfer performances. The taller the reactor, causing longer bubble residence times and thus a prolonged mass transfer process for each bubble, the more relevant this important effect becomes. For a reliable process design, accurate modelling of the effects is, therefore, required.

CRediT authorship contribution statement

Lotta Kursula: Writing – original draft, Visualization, Validation, Software, Methodology, Investigation, Formal analysis, Data curation. **Sayaka Takagi:** Writing – review & editing, Investigation, Formal analysis. **Marko Hoffmann:** Writing – review & editing, Supervision, Project administration, Funding acquisition, Conceptualization. **Felix Kexel:** Writing – review & editing, Supervision, Methodology. **Michael Schlüter:** Writing – review & editing, Supervision, Resources, Project administration, Funding acquisition, Conceptualization.

Declaration of competing interest

The authors declare that they have no known competing financial interests or personal relationships that could have appeared to influence the work reported in this paper.

Acknowledgements

Funded by the Deutsche Forschungsgemeinschaft (DFG, German Research Foundation) - project 501131738.

Data availability

Data is published under the DOI https://doi.org/10.15480/882.17032.

References

[1] S. Matthes, Fundamentals of Microscale Bubbles in Process Engineering 1. Auflage, PhD Thesis, in: Berichte aus dem Institut für Mehrphasenströmungen, Cuvillier Verlag, TUHH, Göttingen, 2021, Number Band 9.

[2] S. Matthes, T. Merbach, J. Fitschen, M. Hoffmann, M. Schlüter, Influence of counterdiffusion effects on mass transfer coefficients in stirred tank reactors, Chem. Eng. J. Adv. 8 (2021) 100180, http://dx.doi.org/10.1016/j.ceja.2021.100180, URL https://www.sciencedirect.com/science/article/pii/S2666821121000958.

[3] L. Kursula, F. Kexel, M. Hoffmann, N.-M. Epping, P. Bubenheim, K. Terasaka, A. Liese, M. Schlüter, Experimental studies on microscopic, multiphase transport phenomena: Novel applications of light sheet fluorescence microscopy, J. Vis. (2026) http://dx.doi.org/10.1007/s12650-026-01115-7.

[4] S. Rehfeldt, J. Stichlmair, Measurement and calculation of multicomponent diffusion coefficients in liquids, Fluid Phase Equilib. 256 (1) (2007) 99–104, http://dx.doi.org/10.1016/j.fluid.2006.10.008, URL https://www.sciencedirect.com/science/article/pii/S0378381206004353.

[5] E.L. Cussler, Diffusion: Mass Transfer in Fluid Systems, Cambridge University Press, 2009.

[6] R. Taylor, R. Krishna, Multicomponent Mass Transfer, Wiley series in chemical engineering, Wiley, New York, 1993.

[7] C. Peters, J. Thien, L. Wolff, H.-J. Koss, A. Bardow, Quaternary diffusion coefficients in liquids from microfluidics and Raman microspectroscopy: Cyclohexane + Toluene + Acetone + Methanol, J. Chem. Eng. Data 65 (2019) http://dx.doi.org/10.1021/acs.jced.9b00632.

[8] G. Guevara-Carrion, R. Fingerhut, J. Vrabec, Fick diffusion coefficient matrix of a quaternary liquid mixture by molecular dynamics, J. Phys. Chem. B 124 (22) (2020) 4527–4535, http://dx.doi.org/10.1021/acs.jpcb.0c01625.

[9] S. Fleckenstein, D. Bothe, A Volume-of-Fluid-based numerical method for multicomponent mass transfer with local volume changes, J. Comput. Phys. 301 (2015) 35–58, http://dx.doi.org/10.1016/j.jcp.2015.08.011, URL https://www.sciencedirect.com/science/article/pii/S0021999115005306.

[10] D. Bothe, P.-É. Druet, On the structure of continuum thermodynamical diffusion fluxes—A novel closure scheme and its relation to the Maxwell–Stefan and the Fick–Onsager approach, Internat. J. Engrg. Sci. 184 (2023) 103818, http://dx.doi.org/10.1016/j.ijengsci.2023.103818, URL https://www.sciencedirect.com/science/article/pii/S0020722523000095.

[11] K. Muroyama, K. Imai, Y. Oka, J. Hayashi, Mass transfer properties in a bubble column associated with micro-bubble dispersions, Chem. Eng. Sci. 100 (2013) 464–473, http://dx.doi.org/10.1016/j.ces.2013.03.043, URL https://www.sciencedirect.com/science/article/pii/S0009250913002273.

[12] F. Karnbach, X. Yang, G. Mutschke, J. Fröhlich, J. Eckert, A. Gebert, K. Tschulik, K. Eckert, M. Uhlemann, Interplay of the open circuit potential-relaxation and the dissolution behavior of a single H2 bubble generated at a Pt microelectrode, J. Phys. Chem. C 120 (28) (2016) 15137–15146, http://dx.doi.org/10.1021/acs.jpcc.6b02305.

[13] S. Hosoda, S. Abe, S. Hosokawa, A. Tomiyama, Mass transfer from a bubble in a vertical pipe, Int. J. Heat Mass Transfer 69 (2014) 215–222, http://dx.doi.org/10.1016/j.ijheatmasstransfer.2013.10.031, URL https://www.sciencedirect.com/science/article/pii/S0017931013008910.

[14] H. Brauer, D. Mewes, Stoffaustausch Einschliesslich Chemischer Reaktionen, Sauerländer, 1971.
[15] L. Kursula, F. Kexel, M. Hoffmann, N.-M. Epping, P. Bubenheim, K. Terasaka, A. Liese, M. Schlüter, Data for publication: Experimental studies on microscopic, multiphase transport phenomena: Novel applications of Light Sheet Fluorescence Microscopy, 2026, http://dx.doi.org/10.15480/882.15833.
[16] L. Kursula, S. Takagi, M. Hoffmann, F. Kexel, M. Schlüter, Data and supplementary information for publication: An experimental study on the time dependence of diffusive mass transfer of single oxygen bubbles, 2026, http://dx.doi.org/10.15480/882.17032.
[17] J.R. Lakowicz, Principles of Fluorescence Spectroscopy, Third edition, corrected at 4. printing, Springer, New York, NY, 2010.
[18] W. Xing, M. Yin, Q. Lv, Y. Hu, C. Liu, J. Zhang, 1 - Oxygen solubility, diffusion coefficient, and solution viscosity, in: W. Xing, G. Yin, J. Zhang (Eds.), Rotating Electrode Methods and Oxygen Reduction Electrocatalysts, Elsevier, Amsterdam, 2014, pp. 1–31, http://dx.doi.org/10.1016/B978-0-444-63278-4.00001-X, URL https://www.sciencedirect.com/science/article/pii/B978044463278400001X.
[19] A. Bardow, V. Göke, H.-J. Koß, K. Lucas, W. Marquardt, Concentration-dependent diffusion coefficients from a single experiment using model-based Raman spectroscopy, PPEPPD 2004 Proceedings, Fluid Phase Equilib. 228–229 (2005) 357–366, http://dx.doi.org/10.1016/j.fluid.2004.08.017, URL https://www.sciencedirect.com/science/article/pii/S0378381204003905.
[20] O.R. Enríquez, C. Sun, D. Lohse, A. Prosperetti, D. Van Der Meer, The quasi-static growth of CO_2 bubbles, J. Fluid Mech. 741 (2014) R1, http://dx.doi.org/10.1017/jfm.2013.667, URL https://www.cambridge.org/core/product/identifier/S0022112013006678/type/journal_article.
[21] Á. Moreno Soto, A. Prosperetti, D. Lohse, D. Van Der Meer, Gas depletion through single gas bubble diffusive growth and its effect on subsequent bubbles, J. Fluid Mech. 831 (2017) 474–490, http://dx.doi.org/10.1017/jfm.2017.623, URL https://www.cambridge.org/core/product/identifier/S0022112017006231/type/journal_article.
[22] Á. Moreno Soto, O.R. Enríquez, A. Prosperetti, D. Lohse, D. Van Der Meer, Transition to convection in single bubble diffusive growth, J. Fluid Mech. 871 (2019) 332–349, http://dx.doi.org/10.1017/jfm.2019.276, URL https://www.cambridge.org/core/product/identifier/S0022112019002763/type/journal_article.
[23] R. Streicher, K. Schügerl, Interchange of fluid mechanics and mass exchange in droplets, Chem. Eng. Sci. 32 (1) (1977) 23–33, http://dx.doi.org/10.1016/0009-2509(77)80191-7, URL https://www.sciencedirect.com/science/article/pii/0009250977801917.
[24] W.K. Lewis, W.G. Whitman, Principles of gas absorption, Ind. Eng. Chem. 16 (12) (1924) 1215–1220, http://dx.doi.org/10.1021/ie50180a002, URL https://pubs.acs.org/doi/abs/10.1021/ie50180a002.
[25] S. Kastens, S. Hosoda, M. Schlüter, A. Tomiyama, Mass transfer from single Taylor bubbles in minichannels, Chem. Eng. Technol. 38 (11) (2015) 1925–1932, http://dx.doi.org/10.1002/ceat.201500065, URL https://onlinelibrary.wiley.com/doi/abs/10.1002/ceat.201500065, _eprint: https://onlinelibrary.wiley.com/doi/pdf/10.1002/ceat.201500065.